

# Searching for charged lepton flavor violation: New results from the MEG experiment

**Gordon Lim**

Department of Physics and Astronomy, University of California, Irvine, California 92697, USA

E-mail: [g.lim@uci.edu](mailto:g.lim@uci.edu)

**Abstract.** Discovery of charged lepton flavor violation would be unambiguous evidence of new physics beyond the Standard Model. The MEG experiment focuses on  $\mu^+ \rightarrow e^+ \gamma$  decay and has recently published a search result based on data collected in 2009 and 2010. No evidence of this decay mode is found in this data sample, resulting in an upper limit on the branching ratio of  $2.4 \cdot 10^{-12}$  at 90% confidence level, the best limit ever achieved for this process. This result as well as the current status and prospects of the MEG experiment are reported here.

## 1. Introduction

Charged lepton flavor violating decays have never been observed. They are highly suppressed in the Standard Model, but many well-motivated theories beyond the Standard Model such as supersymmetric grand unified theories or theories with extra dimensions predict sizable rates up to or even higher than present experimental bounds. Observation of charged lepton flavor violating decay would, therefore, be unambiguous evidence of new physics beyond the Standard Model. The  $\mu \rightarrow e \gamma$  process in particular has been used extensively to search for new physics by many experiments in the past, due to the muon's copious production rate and relatively long lifetime. Anti-muons are used because they are not captured on target nuclei. The MEG collaboration is currently searching for  $\mu^+ \rightarrow e^+ \gamma$  decay with unprecedented sensitivity by using innovative detector technologies and the world's most intense DC surface muon beam at the Paul Scherrer Institute (PSI) near Zurich, Switzerland. The current status, the latest results and the prospects of the MEG experiment are described in the following.

## 2. The MEG experiment

The  $\mu^+ \rightarrow e^+ \gamma$  decay mode at rest is characterized by the simultaneous emission of a back-to-back photon-positron pair in which both particles have an energy equal to half the muon rest mass (52.83 MeV). This signature has two different backgrounds: Radiative muon decays  $\mu^+ \rightarrow e^+ \nu_e \bar{\nu}_\mu \gamma$  (RMD) in which the neutrinos carry away little energy, and accidental coincidences (ACC) of an energetic positron from normal Michel decay  $\mu^+ \rightarrow e^+ \nu_e \bar{\nu}_\mu$  and a gamma-ray coming from RMD, Bremsstrahlung or positron annihilation-in-flight in the materials of the experiment. In the MEG experiment, ACC events dominate the background by more than one order of magnitude. To resolve these backgrounds, a detector with excellent spatial, temporal and energy resolution is required.

The MEG experiment [1] is being conducted at the  $\pi E5$  beam line at PSI, where the world's most intense continuous surface  $\mu^+$  beam of around  $10^8 \mu^+/\text{sec}$  is available. The MEG detector



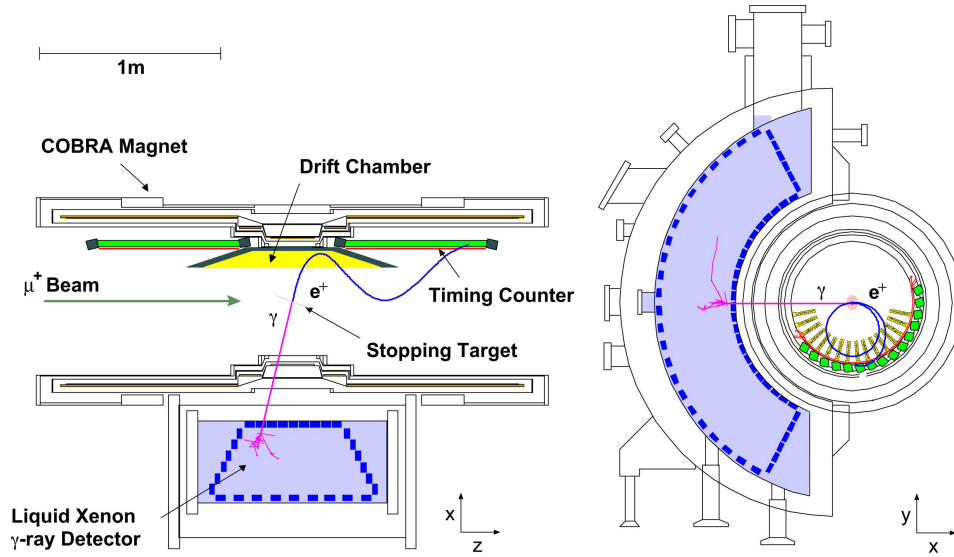


**Figure 1.** Top and front view of the MEG detector.

provides asymmetric coverage ( $\Omega_{\text{MEG}}/4\pi \simeq 11\%$ ) of a retractable 205  $\mu\text{m}$ -thick polyethylene muon stopping target as shown in Figure 1. The detector is composed of a positron spectrometer and a photon detector. The spectrometer is used to measure the positron momentum, direction and timing. It consists of a drift chamber (DC) system flanked by two timing counters (TCs), located inside a superconducting solenoid with a gradient field along the beam axis, ranging from  $\sim 1.3$  T at the center to  $\sim 0.5$  T at either end. A gradient field is employed to cancel the dependence of the positron bending radius on the emission angle, and to efficiently sweep out low energy positrons from the spectrometer volume. The solenoid is filled with helium and has a fiducial thickness of  $0.2 X_0$ . The DC system consists of 16 radially staggered double-layer modules, where each layer contains 9 axial drift cells equipped with very thin Vernier cathode pads. The counting gas in the DC modules is a 50%-50% mixture of helium and ethane. The total radiation length along positron trajectories is  $\sim 2 \cdot 10^{-3} X_0$  due to the open-frame DC module design. Each TC consists of 15 axial scintillation bars read out by PMTs, and 128 semi-circular scintillation fibers read out by APDs. The photon detector, located outside of the solenoid, is a homogeneous volume (900 l) of liquid xenon (LXe) viewed by 846 UV-sensitive PMTs submerged in the LXe. It is used to reconstruct the photon energy as well as the position and time of its first interaction in the LXe. The LXe scintillation process is used because of the fast response ( $\tau_{\text{decay}} = 45$  ns), the high stopping power ( $X_0 = 2.8$  cm) and the absence of self-absorption ( $\lambda_{\text{abs}} > 1$  m). The cathode area coverage of the photon detector is about 40%, its total stopping power is about  $14 X_0$ . All detector signals are individually digitized by in-house designed waveform digitizers based on the multi-GHz domino ring sampler chip (DRS) [2]. Candidate  $\mu^+ \rightarrow e^+ \gamma$  events are triggered by the presence of a high energy gamma-ray in the LXe detector and a hit in one of the TCs within a 20 ns window, together with an approximate back-to-back topology. Pre-scaled monitoring and calibration triggers are also recorded. The data acquisition system is based on the MIDAS software package, the online and offline data analysis are done with a common analyzer based on the framework generator ROME [3].

The MEG detector response, resolutions and stability are constantly monitored and calibrated during data acquisition using various calibration and monitoring tools. The gains and quantum-efficiencies of the photon detector PMTs are calibrated and monitored daily by a lattice of 44 LEDs and 25 point-like Am  $\alpha$ -sources immersed in the LXe. The energy response of the photon

detector is calibrated and monitored using gamma-rays from various sources. A radioactive Am/Be source and a pulsed and triggerable neutron generator are used twice per week to produce 4.4 and 9 MeV gamma-rays, respectively. A dedicated Cockcroft-Walton accelerator is also used twice per week to direct protons from the down-stream side of the detector on a lithium tetraborate target, producing monochromatic 17.6 MeV gamma-rays and a coincident gamma-ray pair of 4.4 and 11.6 MeV. Once per year negative pions are collected by the  $\pi E5$  beam line and directed on a liquid hydrogen target to generate  $\pi^-p$  charge exchange and radiative capture reactions that produce 54.9, 82.9 and 129 MeV gamma-rays. The spectrometer is calibrated and aligned using cosmic rays and positrons from Michel decays. The response of the spectrometer is determined using Michel positrons that make two spiral turns in the DC system. The relative timing between the photon detector and the TCs is calibrated using RMD events and coincident gamma-ray pairs generated by the Cockcroft-Walton accelerator.

### 3. Detector performance

The MEG experiment has been taking data since 2008. The collaboration has recently published its results based on data collected in 2009 and 2010<sup>1</sup> [4]. All sub-detectors were running stably during these periods. The total number of  $\mu^+$ -decays in the target in these data sets corresponds to  $\sim 0.7 \cdot 10^{14}$  and  $\sim 1.1 \cdot 10^{14}$ , respectively. The detector resolutions, parameterized in terms of Gaussians distribution widths, are listed in Table 1. The  $(x, y, z)$  coordinate system is defined as in Figure 1. The  $\theta$  and  $\phi$  angles are the polar and azimuthal angles with respect to the beam direction. The photon detector coordinates  $u$  and  $v$  coincide with  $z$  and  $r\phi$ , while  $w$  is the distance from the inner wall of the LXe volume. The trigger efficiencies and the reconstruction efficiencies within the detector acceptance are also listed in Table 1.

**Table 1.** MEG detector performance during 2009 and 2010.

Resolution	2009	2010
$\gamma$ energy	1.9% ( $w > 2$ cm), 2.4% ( $w < 2$ cm)	1.9% ( $w > 2$ cm), 2.4% ( $w < 2$ cm)
$\gamma$ position	5 mm ( $u, v$ ), 6 mm ( $w$ )	5 mm ( $u, v$ ), 6 mm ( $w$ )
$e^+$ momentum	0.74% (80% core fraction)	0.74% (79% core fraction)
$e^+$ angles	9.4 mrad ( $\theta$ ), 6.7 mrad ( $\phi$ )	11 mrad ( $\theta$ ), 7.2 mrad ( $\phi$ )
$e^+$ vertex	1.5 mm ( $z$ ), 1.1 mm ( $y$ )	2.0 mm ( $z$ ), 1.1 mm ( $y$ )
$\gamma$ - $e^+$ timing	146 ps	122 ps
Efficiency		
trigger	91%	92%
$\gamma$ reconstruction	58%	59%
$e^+$ reconstruction	40%	34%

In 2010 a DRS upgrade resulted in an improvement in the time resolution while an increase in noise in the DC system, due to a deterioration of the high-voltage power supplies, and some unusable DC modules caused a slightly worse positron tracking performance.

<sup>1</sup> The 2008 data are not used due to their limited statistics and detector performance [5].

#### 4. Analysis procedure

Several improvements to the analysis have been introduced since the presentation of the preliminary result based on the 2009 data [6]. These improvements include a new alignment technique for the DC system and the relative alignment of the photon detector and the spectrometer, a better understanding of the gradient magnetic field map, an improved spectrometer performance evaluation and an improved likelihood analysis method.

The observables used to identify  $\mu^+ \rightarrow e^+\gamma$  decays are the relative time between the photon and the positron ( $t_{e\gamma}$ ), the polar and azimuthal angles between the two particles ( $\theta_{e\gamma}$ ,  $\phi_{e\gamma}$ ) and their energies ( $E_\gamma$ ,  $E_e$ ). We adopt a likelihood analysis method combined with a blinding procedure: events that fall into a pre-defined blinding window that contains the signal region are saved in separate hidden data files until the analysis procedure is completely defined. The blind region is defined by  $48 < E_\gamma < 58$  MeV and  $|t_{e\gamma}| < 1$  ns. Events outside of this window (side-bands) are used for optimizing the analysis parameters, studying the background and, finally, constructing the probability density functions (PDFs) needed for the likelihood analysis.

A likelihood analysis is carried out for events in a portion of the blind region defined by  $48 < E_\gamma < 58$  MeV,  $50 < E_e < 56$  MeV,  $|t_{e\gamma}| < 0.7$  ns,  $|\theta_{e\gamma}| < 50$  mrad and  $|\phi_{e\gamma}| < 50$  mrad. These intervals are between five and twenty sigmas wide to fully contain the signal events and also retain some background events. The best estimates of the numbers of signal, RMD and ACC events in the analysis region are obtained by maximizing the following likelihood function:

$$\begin{aligned} \mathcal{L}(N_{\text{sig}}, N_{\text{RMD}}, N_{\text{ACC}}) &= \frac{e^{-N}}{N_{\text{obs}}!} e^{-\frac{(N_{\text{RMD}} - \langle N_{\text{RMD}} \rangle)^2}{2\sigma_{\text{RMD}}^2}} e^{-\frac{(N_{\text{ACC}} - \langle N_{\text{ACC}} \rangle)^2}{2\sigma_{\text{ACC}}^2}} \\ &\times \prod_{i=1}^{N_{\text{obs}}} (N_{\text{sig}} S(\vec{x}_i) + N_{\text{RMD}} R(\vec{x}_i) + N_{\text{ACC}} A(\vec{x}_i)) \end{aligned}$$

where  $\vec{x}_i = \{E_\gamma, E_e, t_{e\gamma}, \theta_{e\gamma}, \phi_{e\gamma}\}$  is the vector of observables for the  $i$ -th event.  $N_{\text{sig}}$ ,  $N_{\text{RMD}}$  and  $N_{\text{ACC}}$  are the fitted number of signal, RMD and ACC events, while  $S$ ,  $R$  and  $A$  are their corresponding PDFs. The PDFs are constructed from the measured detector response functions and the background spectra observed in the side-bands. The dependence of the resolutions on the position of the gamma-ray conversion point and on the quality of the positron track reconstruction are taken into account in the likelihood function on an event-by-event basis.  $N_{\text{obs}}$  is the observed number of events, and  $N = N_{\text{sig}} + N_{\text{RMD}} + N_{\text{ACC}}$ . The two Gaussian terms are the constraints on the numbers of RMD and ACC events, where  $\langle N_{\text{RMD}} \rangle$  and  $\langle N_{\text{ACC}} \rangle$  are the expected numbers of RMD and ACC events in the analysis window, while  $\sigma_{\text{RMD}}$  and  $\sigma_{\text{ACC}}$  are the corresponding uncertainties. These are estimated by extrapolating the number of RMD and ACC events observed in the side-bands, resulting in  $\langle N_{\text{RMD}} \rangle \pm \sigma_{\text{RMD}} = 27.2 \pm 2.8$  ( $52.2 \pm 6.0$ ) and  $\langle N_{\text{ACC}} \rangle \pm \sigma_{\text{ACC}} = 270.9 \pm 8.3$  ( $610.8 \pm 12.6$ ) for the 2009 (2010) data set.

The computation of the confidence interval on  $N_{\text{sig}}$  is based on a frequentist approach with a profile likelihood-ratio ordering [7] [8], where  $N_{\text{RMD}}$  and  $N_{\text{ACC}}$  are profiled as

$$\lambda_p(N_{\text{sig}}) = \frac{\mathcal{L}(N_{\text{sig}}, \hat{N}_{\text{RMD}}(N_{\text{sig}}), \hat{N}_{\text{ACC}}(N_{\text{sig}}))}{\mathcal{L}(\hat{N}_{\text{sig}}, \hat{N}_{\text{RMD}}, \hat{N}_{\text{ACC}})}$$

where the hat and double hat denote the best estimates maximizing the likelihood for floating and fixed  $N_{\text{sig}}$ , respectively. Other, independent analysis schemes based on averaged PDFs without event-by-event information or using a Bayesian approach were also used and found to be compatible with the analysis presented here to within 10 to 20% difference in the obtained branching ratio upper limits.

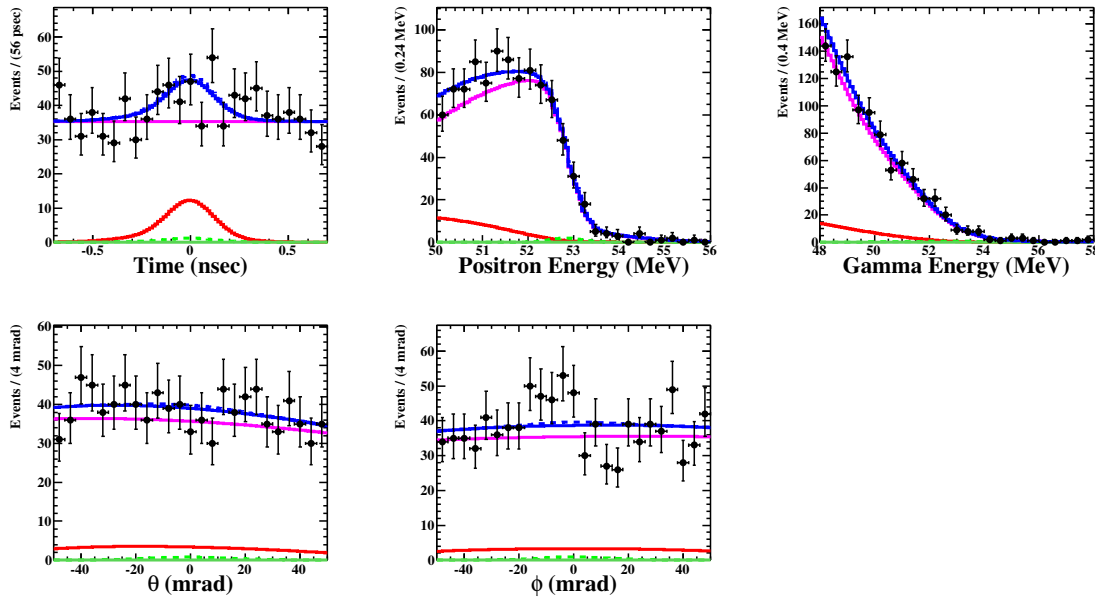


**Figure 2.** Distributions of the five observables  $t_{e\gamma}$ ,  $E_e$ ,  $E_\gamma$ ,  $\theta_{e\gamma}$  and  $\phi_{e\gamma}$  in the analysis region. Projections of the fitted PDFs  $S$  (green),  $R$  (red),  $A$  (magenta) and their total (blue) are shown as colored lines. The dotted lines include the upper limit on  $N_{\text{sig}}$  at 90% C.L. for comparison.

In order to convert  $N_{\text{sig}}$  into a branching ratio value, the normalization relative to the Michel decay is computed by counting the number of Michel positrons that pass the same selection criteria. This is accomplished by means of a pre-scaled Michel positron trigger enabled during data acquisition, to eliminate the dependence on variations in the beam rate or detector conditions. An alternative, independent normalization is calculated using RMD events in the  $E_\gamma$  side-band combined with the theoretical RMD branching ratio. Both methods are in good agreement and are combined to give the normalization factor with a 7% uncertainty.

The sensitivity of the experiment with a null signal hypothesis is defined as the median of the distribution of upper limits on the branching ratio at 90% confidence level (C.L.) obtained over an ensemble of toy MC experiments, taking into account the number of RMD and ACC events as measured in the side-bands. The sensitivity of the 2009 + 2010 data sample is calculated to be  $1.6 \times 10^{-12}$ , and is consistent with the branching ratio upper limits derived from the side-bands demonstrating a good control over the background description.

## 5. Results

The distributions of the five observables in the analysis region and the projected maximum likelihood fit results are shown in Figure 2. The maximum likelihood estimate for the number of signal, RMD and ACC events in the analysis region yields  $N_{\text{sig}} = -0.5^{+7.9}_{-4.7}$ ,  $N_{\text{RMD}} = 76.5 \pm 12$  and  $N_{\text{ACC}} = 882 \pm 22$ , respectively, while  $N_{\text{obs}} = 956$ . Some 2-dimensional event distributions are shown in Figure 3.

No significant excess was found in the data set, resulting in an upper limit on the number of signal events. The corresponding upper limit on the branching ratio is  $2.4 \cdot 10^{-12}$  at 90% C.L.. The systematic uncertainties of the PDF parameters and the normalization factor are taken into account in the calculation of the upper limit by varying the PDFs according to the uncertainties.

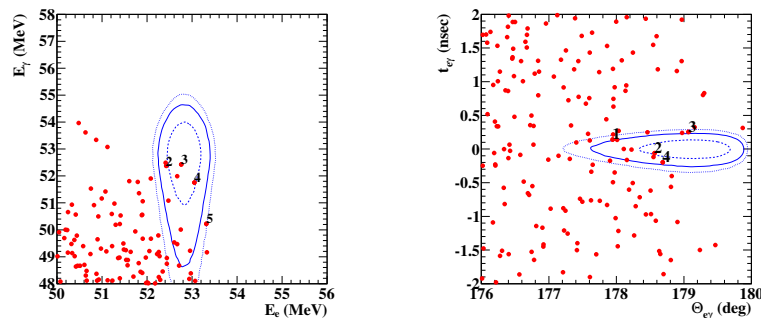


**Figure 3.** Event distribution in the  $E_e - E_\gamma$  and the  $\Theta_{e\gamma} - t_{e\gamma}$  plane, where  $\Theta_{e\gamma}$  is defined as the angle between the positron and the photon. For each 2-dimensional projection, a 90% signal efficiency selection is applied on the other two observables. The  $1\sigma$ ,  $1.64\sigma$  and  $2\sigma$  contours of the 2-dimensional projections of the signal PDF are shown as blue dashed, solid, and dotted lines. Events with the highest relative signal likelihood are numbered.

The largest contributions to the systematic uncertainty come from the uncertainties of the offsets of the relative angles, the correlations in the positron observables and the normalization. The total shift in the branching ratio upper limit amounts to about 2%.

## 6. Summary and outlook

The MEG experiment searches for charged lepton flavor violating  $\mu^+ \rightarrow e^+\gamma$  decay with an unprecedented sensitivity. The result of the analysis on the data acquired in 2009 and 2010 is recently published. No evidence of  $\mu^+ \rightarrow e^+\gamma$  decay is found in the analysis of this data sample, leading to an upper limit on the branching ratio of the  $\mu^+ \rightarrow e^+\gamma$  mode of  $2.4 \cdot 10^{-12}$  at 90% C.L.. This constitutes the most stringent limit on the existence of  $\mu^+ \rightarrow e^+\gamma$  decay, improving the previous best limit by a factor of five [9].

During 2011, the MEG experiment collected a data sample comparable to the 2009 + 2010 statistics. Data acquisition is currently ongoing and, since the improvement in sensitivity is slowed down by the backgrounds, is planned to finish in the present detector configuration in 2013. The detector performance is expected to be similar or slightly better than in 2010, resulting in a final sensitivity in the  $10^{-13}$  region. Various detector upgrades are currently under discussion that could improve this sensitivity by another order of magnitude in the near future. Proposed upgrades include an enlarged single volume DC or time-projection chamber, smaller photo-sensors on the inner wall of the LXe volume, the replacement of the current TC system by a lattice of small scintillating tiles, an active target and a silicon vertex tracker.

## References

- [1] Baldini A, Mori T *et al.* 2010 MEG Proposal to PSI, available at <http://meg.psi.ch/docs>
- [2] Ritt S *et al.* 2010 *Nucl. Instr. and Meth.* **A 623** 486
- [3] Cattaneo P W *et al.* 2011 *Eur. Phys. J. Plus* **126** 60
- [4] Adam J *et al.* (MEG Collaboration) 2011 *Phys. Rev. Lett.* **107** 171801
- [5] Adam J *et al.* (MEG Collaboration) 2010 *Nucl. Phys.* **B834** 1
- [6] Sawada R for the MEG collaboration, talk presented at ICHEP2010, 35th International Conference on High Energy Physics, July 22nd-28th, 2010, Paris, France. Proceedings: PoS (ICHEP2010) 263
- [7] Nakamura K *et al.* (Particle Data Group) 2010 *J. Phys.* **G37** 075021
- [8] Feldman G J and Cousins R D 1998 *Phys. Rev.* **D57** 3873
- [9] Brooks M L *et al.* (MEGA Collaboration) 1999 *Phys. Rev. Lett.* **83** 1521